Misfit Accommodation in a Quenched and Aged Al-Cu Alloy with Silicon Particles

M.J. STARINK, P. VAN MOURIK, and B.M. KOREVAAR

Quenched and aged specimens of the Al-1.3 at. pct Cu-19.1 at. pct Si alloy were studied by X-ray diffraction. Since this alloy contains a high volume percentage (~20 vol pct) of second-phase Si particles, it is regarded as a model for a metal matrix composite (MMC). During isothermal aging of the solid-quenched Al-1.3 at. pct Cu-19.1 at. pct Si alloy, the Cu and Si atoms precipitate. This causes the Al-rich phase lattice parameter to increase from a value lower to a value higher than the lattice parameter of pure unstrained aluminum. Due to thermal misfit after quenching from heat-treatment temperatures, all lattice parameters are influenced by residual stresses. A model describing the elastic/plastic accommodation of a misfitting spherical inclusion in an infinite matrix is adapted for the case of misfitting inclusions in a finite matrix. This model describes the measured lattice parameter shifts of the Si phase reasonably well. Comparison of the model for elastic accommodation and the model for elastic/plastic accommodation with measured stresses shows significant discrepancies for the low-temperature range ($\Delta T < 200$ K). These discrepancies may be related to the volume effect of defects (dislocations, vacancies) created in the plastic zone.

I. INTRODUCTION

RAPID solidification of aluminum alloys with a high percentage of silicon (about 20 at. pct) yields finely grained microstructures with a fine dispersion of silicon particles.[1] By consolidation of the rapidly solidified ribbons or powders, aluminum alloys with improved mechanical properties as compared to conventional aluminum alloys can be produced. These improved properties, *e.g.*, increased wear resistance and reduced thermal expansion,[2] make these alloys attractive for applications like parts of combustion engines. In many aspects, *e.g.*, volume fraction, size, and thermal expansion of dispersed particles, the rapidly solidified aluminum alloys with a large silicon content resemble particulate-reinforced metal matrix composites (MMCs). Hence, these alloys are considered as *in situ* composites.

The presence of reinforcing particles can influence the kinetics of precipitation in aluminum alloys.[3–6] This influence is usually explained as follows. The difference in shrinkage on cooling, due to the difference in the respective coefficients of thermal expansion (CTE) of the dispersed particles and the surrounding matrix, introduces a thermal misfit between particles and matrix. This thermal misfit is accommodated by elastic and plastic deformation of the matrix,[7] the latter implying creation of dislocations. These act as extra nucleation sites (enhancing precipitation) or annihilate excess vacancies (retarding precipitation). Elastic stresses resulting from misfit accommodation can also influence precipitation phenomena.[8]

The Al-1.3 at. pct Cu-19.1 at. pct Si model alloy produced by melt spinning and subsequent extrusion combines the attractive mechanical properties of aluminum alloys with a large silicon content with the possibility of age hardening of the matrix. The combination of a heat-treatable Al matrix with the presence of silicon particles allows the study of important effects in MMCs, such as thermal stresses and precipitation. The nonisothermal precipitation in the solid-quenched Al-1.3 at. pct Cu-19.1 at. pct Si alloy was studied before.[9] In the present work, the isothermal aging in the solid-quenched Al-1.3 at. pct Cu-19.1 at. pct Si alloy is studied by measurement of lattice parameter variations of the Al-rich and Si-rich phases.

II. EXPERIMENTAL PROCEDURES

A. *Preparation of Specimens*

A high-purity Al-1.3 at. pct Cu-19.1 at. pct Si alloy was produced by melt spinning and subsequent extrusion. The production route of the alloy was described earlier.[9] In the extruded alloy, the Si particle size is about 0.5 to 1 μm.[9] From the center of the extruded bars, cylindrical specimens were machined with a diameter of 0.5 mm and length of about 5 mm. The axis of the specimen was parallel to the extrusion direction. These specimens were intended for X-ray diffraction experiments with a Debije-Scherrer (DbS) camera.

The specimens were solution treated for 5 minutes at 793 K in a vertical tube furnace and subsequently quenched in water at room temperature. An optical micrograph of a solution-treated specimen (Figure 1) shows that the Si particles are approximately spherical with sizes of about 1 to 2 μm. The grain size of the Al-rich phase is about 10 μm. A part of the specimens was stored at room temperature awaiting further experiments. Another part of the specimens was stored in liquid nitrogen. The corresponding indications are SQ/RT and SQ/LN, respectively. The quenched specimens were aged at 423, 453, and 483 K. The quenched and aged specimens are indicated as SQ + A specimens, followed by the aging temperature. The aging treatment

M.J. STARINK, Scientist, and P. VAN MOURIK, Senior Scientist, are with the Laboratory of Metallurgy, Delft University of Technology, 2628 AL Delft, The Netherlands. B.M. KOREVAAR, Retired Professor, Laboratory of Metallurgy, Delft University of Technology.

Manuscript submitted July 6, 1992.

was performed in an oil bath with temperature stability ±1.5 K and was terminated by a direct quench into water at room temperature.

To study the effect of specimen size on the Al-rich phase lattice parameter after quenching, a melt-spun ribbon (thickness ~50 μm) was aged for 700 hours at 423 K and subsequently quenched in water at room temperature. This liquid-quenched and aged specimen will be referred to as LQ + A423.

To study the effect of dissolved Cu and Si atoms on the Al-rich phase lattice parameter in the absence of Si particles, an Al-1.07 at. pct Cu-1.01 at. pct Si alloy was produced from 99.999 pct pure Al, 99.99 pct pure Si, and a 99.95 pct pure Al-50 pct Cu master alloy (all percentages by weight) by conventional casting. The ingot was homogenized at 798 K for 5 days and subsequently quenched in water at room temperature. Filings were prepared from a slice cut from the ingot. These filings were collected in a quartz tube, homogenized for 2 hours at 798 ± 2 K, and subsequently quenched in water at room temperature.

B. *X-ray Diffraction*

For measurement of the lattice parameter of the Al-rich and Si-rich phases of the Al-1.3 at. pct Cu-19.1 at. pct Si alloy, X-ray diffraction experiments were performed using a DbS camera. Unfiltered copper radiation was used. Exposure time for the films was 3 hours. During the exposure, the temperature inside the DbS camera at a point close to the specimen was measured and recorded. Temperatures during the exposures were between 294 and 297 K. Temperature variations during single experiments were typically about 0.5 K. Film type and development procedures were identical for all experiments.

For each reported lattice parameter value, a single DbS diffraction experiment was performed. Accuracy of the line position measurements of the two lines corresponding to the highest diffraction angle was improved by taking the average of at least five determinations of their positions. The lattice parameters of the Al-rich and Si-rich phases were determined using the Nelson-Riley extrapolation[10] and were corrected for the average temperature during the exposure by adopting the CTE of pure aluminum and pure silicon: 23.5 10^{-6} and 3 10^{-6}, respectively.[11] All lattice parameters presented in this work are valid at 298 K.

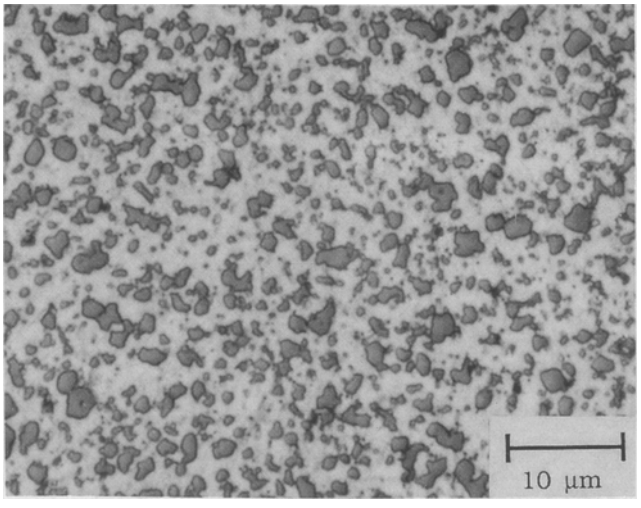

Fig. 1—Optical micrograph of an SQ Al-1.3 at. pct Cu-19.1 at. pct Si specimen.

III. RESULTS

The Al-rich and the Si-rich phases were always detected. The DbS experiments showed some variations of intensity of the diffracted Al lines. This is evidence of a weak (extrusion) texture. In some cases, lines from the θ and/or θ' phases (both Al_2Cu) were also observed. No other phases were observed for any of the specimens. For the as-extruded (AE) specimens, the θ phase was the only intermetallic phase observed. For SQ specimens, no intermetallic phase was observed. On artificial aging, the lines diffracted by the Al_2Cu phases appear after certain times. After an Al_2Cu phase has been detected, it remains present at subsequent aging times studied. In Table I, the minimum aging times for the appearance of the Al_2Cu phases in SQ + A specimens are given. The lattice parameters of the Al-rich and the Si-rich phases in AE and SQ specimens are gathered in Table II. It is observed that the Si-rich phase lattice parameter after quenching and storage in liquid nitrogen (SQ/LN) is much larger than after quenching and storage at room temperature (SQ/RT). The Al-rich phase lattice parameter after SQ/LN is somewhat lower than after SQ/RT. For the AE specimen, the lattice parameter of the Al-rich phase is within the experimental error equal to the value for pure, unstrained aluminum (0.40496 nm[12]).

To obtain a reference value for the lattice parameter of pure, unstrained silicon, the lattice parameter of pure

Table I. Minimum Aging Times, t_m, Required for the Appearance of Lines Diffracted by the Al_2Cu Phases in SQ+A Al-1.3 At. pct Cu-19.1 At. pct Si Specimens

	SQ + A 423 K t_m (Hours)	SQ + A 453 K t_m (Hours)	SQ + A 483 K t_m (Hours)
θ'	8	3.5	2
θ	512	128	16

Table II. Lattice Parameters of the Al-Rich and Si-Rich Phases (a_{Al} and a_{Si}, Respectively) in an AE and four SQ Al-1.3 At. pct Cu-19.1 At. pct Si Specimens*

Specimen	a_{Al} (nm)	a_{Si} (nm)
AE	0.40495 ± 0.00002	0.54284 ± 0.00003
SQ/LN1	0.40417 ± 0.00004	0.54306 ± 0.00003
SQ/LN2	0.40422 ± 0.00003	0.54293 ± 0.00002
SQ/RT1	0.40431 ± 0.00003	0.54254 ± 0.00005
SQ/RT2	0.40426 ± 0.00003	0.54254 ± 0.00003

*The SQ specimens were either stored at room temperature after quenching (RT) or in liquid nitrogen (LN).

silicon (NBS SRM 640 powder) was determined twice. This yielded $a^{\circ}_{Si} = 0.54308 \pm 0.00001$ nm. The measured lattice parameters of the Si-rich phase in the Al-1.3 at. pct Cu-19.1 at. pct Si alloy are in all cases smaller than this value.

The lattice parameters of the Al-rich and the Si-rich phases as a function of aging time are presented in Figures 2 and 3. It is observed that during aging at 483 K, the Al-rich phase lattice parameters obtained from specimens stored at room temperature coincide with the ones obtained from specimens stored in liquid nitrogen. Thus, the difference in storage temperature between quenching and aging has no significant effect on the kinetics of aging at 483 K. Also, the Si-rich phase lattice parameter during aging at 483 K is not significantly influenced by the difference in storage temperature. During aging, the Al-rich phase lattice parameter increases from values around 0.4042 nm to about 0.4051 nm. This last value is significantly larger than the value for pure, unstrained Al (0.40496 nm). During aging, the Si-rich phase lattice parameter remains approximately constant. It is observed that the lattice parameter of the Si-rich phase decreases with increasing aging temperature.

The DbS experiment on the aged melt-spun ribbon LQ+A423 yielded an Al-rich phase lattice parameter of 0.40516 ± 0.00002 nm. Besides Al-rich phase lines, only Si-rich phase lines and θ phase lines were observed.

The DbS experiment on the conventionally cast, homogenized, and solid-quenched Al-1.07 at. pct Cu-1.01 at. pct Si alloy yielded for the Al-rich phase lattice parameter 0.40428 ± 0.00001 nm. Only lines diffracted from the Al-rich phase were observed.

IV. DISCUSSION

A. *Misfit Stresses for a Spherical Inclusion Embedded in a Plastically Deforming, Finite Matrix*

As the misfitting Si particles are mostly equiaxed and approximately spherical (Figure 1), a model for misfitting spherical particles will be used to explain observed misfit strains. For a spherical inclusion B in a continuous matrix phase A, the misfit parameter ϵ is defined as

$$\varepsilon = \frac{r_B^0 - r_A^0}{r_A^0} \quad [1]$$

where r_B^0 and r_A^0 are the radii of the free undeformed inclusion B and the empty undeformed cavity in the matrix A, respectively. For the case of thermal misfit (misfit due to a temperature change, ΔT), the misfit parameter is given by

$$\varepsilon = (\alpha_A - \alpha_B)\Delta T \quad [2]$$

where α_A and α_B are the coefficients of thermal expansion of matrix and inclusion, respectively. In the following, we consider the case of a positive misfit parameter, *i.e.*, $r_B^0 > r_A^0$. For the case of a negative misfit parameter, similar formulas can be derived. For the case of elastic accommodation of misfit in an infinite elastically isotropical matrix, the inclusion (also assumed elastically isotropical) will be in a state of hydrostatic compression. The pressure inside the inclusion for an infinitely small volume fraction of inclusions is given by[13]

$$p_B = 3K_B\,(C - 1)\varepsilon \quad [3]$$

with

$$C = \frac{3K_B}{3K_B + 4\mu_A} \quad [4]$$

where μ is the shear modulus and K is the bulk modulus. (Note that since $C < 1$, p_B is negative.)

For a finite matrix, it is required that the surface of the matrix be traction free, *i.e.*, that the stresses normal to the surface be zero. The boundary condition requiring that $\sigma_r = 0$ on the surface of the matrix, is equivalent to requiring that on any plane through the finite specimen, the compressive stress in the inclusion is balanced

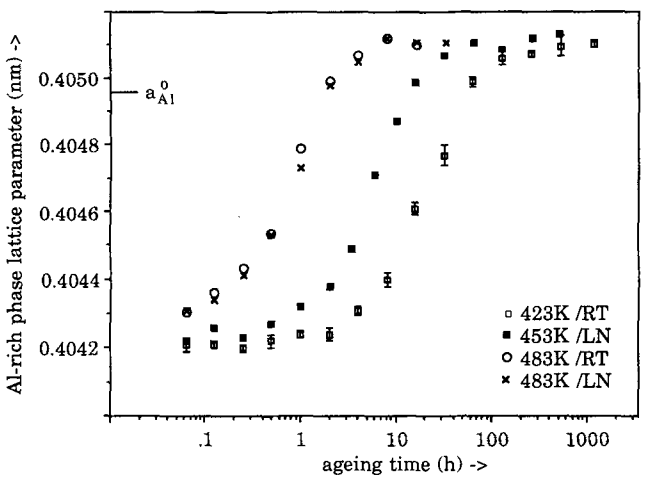

Fig. 2—The Al-rich phase lattice parameters of Al-1.3 at. pct Si specimens as a function of time of aging at the indicated temperatures; storage between quenching and aging was at room temperature (RT) or in liquid nitrogen (LN). The lattice parameter for pure, unstrained aluminum, a°_{Al}, is indicated.

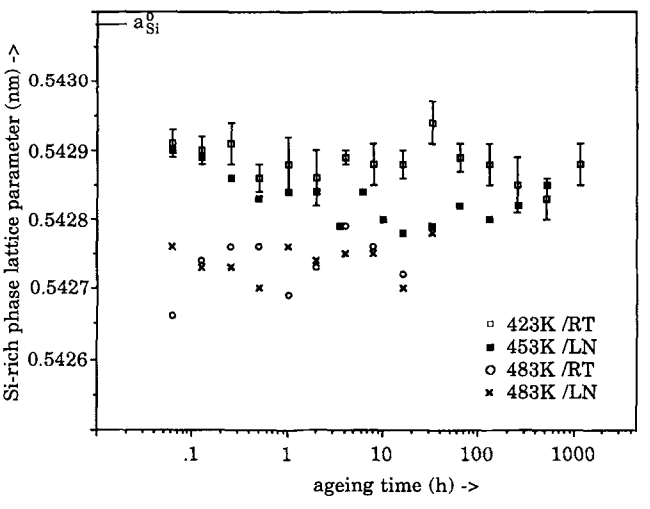

Fig. 3—The Si-rich phase lattice parameter of Al-1.3 at. pct Cu-19.1 at. pct Si specimens as a function of time of aging at the indicated temperatures; storage between quenching and aging was at room temperature (RT) or in liquid nitrogen (LN). The lattice parameter for pure, unstrained silicon, a°_{Si}, is indicated.

by tensile stresses in the matrix. In a spherically symmetric case, this can be obtained from the solution of the stresses in the infinite matrix by adding a uniform hydrostatic stress. This balancing stress is usually termed the image stress, p^i. Assuming that the stress state in the inclusions is not disturbed by interaction of stress fields, the balance of forces requires

$$p^i + y_B p_B = 0 \qquad [5]$$

where yB is the volume fraction of inclusions. (Note that p^i is positive and hence represents a hydrostatic tension.)

Lee *et al.*[14] calculated the stress state in the case of a spherical misfitting inclusion in an infinite matrix which deforms plastically around an inclusion. In their model, the matrix is assumed to be a perfectly plastic material (nonstrain hardening), the flow stress-strain behavior is assumed to be independent of strain rate and of stress orientation, and both inclusion and matrix are assumed to be isotropic. The von Mises yielding criterion is used. This criterion states that yielding occurs when an equivalent stress, σ_e, exceeds the yield stress, σ_y, where σ_e is given by (using polar coordinates)

$$\sigma_e = \frac{1}{\sqrt{2}}[(\sigma_r - \sigma_\theta)^2 + (\sigma_\varphi - \sigma_\theta)^2 + (\sigma_\varphi - \sigma_r)^2]^{1/2} \qquad [6]$$

For the case of a spherically symmetrical stress state, this equation is reduced to

$$\sigma_e = |\sigma_r - \sigma_\theta| \qquad [7]$$

Lee *et al.*[14] obtained the following expressions for the stress components in the inclusion, in the plastically deformed matrix, and in the elastically deformed matrix, respectively:

$$\sigma_r = \sigma_\theta = p_B \quad r < a \qquad [8a]$$

$$\sigma_r = \sigma_\theta - \sigma_y = 2\sigma_y \ln\left(\frac{r}{a}\right) + p_B \quad a \le r \le r_p \qquad [8b]$$

$$\sigma_r = -2\sigma_\theta = -\frac{2}{3}\sigma_y \left(\frac{r_p}{r}\right)^3 \quad r > r_p \qquad [8c]$$

where r_p is the radius of the plastically deformed zone and a is the radius of the inclusion. Thus, the inclusion is in a state of uniform hydrostatic compression. Since the stresses at the plastic front must be continuous, it follows that

$$r_p = a \exp\left[-\frac{p_B}{2\sigma_y} - \frac{1}{3}\right] \qquad [9]$$

From the spherical symmetry, it follows that the displacements are all radial.[14] Hence, it is not necessary to assume either a coherent or a noncoherent interface. Continuity conditions of displacements and radial stresses at the precipitate/matrix interface yield an expression from which pB can be evaluated:

$$\frac{6\eta\mu\varepsilon}{\sigma_y}\left[1 + \frac{p_B}{3K_B\varepsilon} - \frac{p_B}{3K_A\varepsilon}\right] = \exp\left[-\frac{3p_B}{2\sigma_y} - 1\right] \qquad [10]$$

where $\eta = (1 + \nu)/3(1 - \nu)$ (ν is Poisson's ratio of the matrix).

Now consider the case of a spherical inclusion with radius a in a spherical matrix with radius R. From the spherical symmetry follows that in this finite specimen, the radial components of the stresses are obtained by adding the image stress, p^i, to the stresses in the case of the finite matrix:

$$\sigma_r = p_B + p^i \quad r < a \qquad [11a]$$

$$\sigma_r = 2\sigma_y \ln\left(\frac{r}{a}\right) + p_B + p^i \quad a \le r \le r_p \qquad [11b]$$

$$\sigma_r = -\frac{2}{3}\sigma_y \left(\frac{r_p}{r}\right)^3 + p^i \quad r > r_p \qquad [11c]$$

Since the boundary equation requires that $\sigma_r = 0$ on the surface, the image stress can directly be obtained from Eqs. [11b] and [11c]:

$$p^i = -p_B - 2\sigma_y \ln\left(\frac{R}{a}\right) \quad R < r_p \qquad [12a]$$

$$p^i = \frac{2}{3}\sigma_y \left(\frac{r_p}{R}\right)^3 \quad R \ge r_p \qquad [12b]$$

The volume fraction of precipitates can be substituted for the ratio a/R:

$$y_B = \left(\frac{a}{R}\right)^3 \qquad [13]$$

and the combination of Eqs. [9], [10], [12], and [13] gives the image stress in a composite with a spherical inclusion.

Finally, it is assumed that the average image stress in a multiparticle composite equals the image stress obtained previously for a one-particle composite.

B. *Influence of Dissolved Atoms and Thermal Misfit Stresses on Lattice Parameters*

For both homogeneous Al-Si and homogeneous Al-Cu alloys, the lattice parameter of the Al-rich phase, a_{Al}, is proportional to the fraction of alloying atoms dissolved in the Al-rich phase, x_{Si} and x_{Cu}.[13,15] Since in many ternary alloy systems the lattice parameter can be calculated from binary data using additive relationships,[16] it is assumed that the effects of both alloying elements are independent and additive; *i.e.*

$$\frac{\Delta a^d_{Al}}{a^\circ_{Al}} = p_{Si}x_{Si} + p_{Cu}x_{Cu} \qquad [14]$$

where a°_{Al} is the lattice parameter of pure unstrained aluminum, Δa^d_{Al} is the lattice parameter shift due to dissolved atoms, and p_{Si} and p_{Cu} are the Vegard constants for Si and Cu atoms dissolved in the Al-rich phase, respectively ($p_{Si} = -4.30\ 10^{-2}$[13] and $p_{Cu} = -1.18\ 10^{-1}$[15]). The assumption of additivity can be checked for the homogenized Al-1.07 at. pct Cu-1.01 at. pct Si alloy. For this alloy, it was found that $a_{Al} = 0.40428 \pm 0.00001$ nm. Applying Eq. [14], one finds a_{Al} =

0.404273 nm. Hence, it is concluded that the effects of Si and Cu atoms dissolved in the Al-rich phase are indeed additive.

At the solution-treatment temperature applied to the ternary Al-Cu alloy with silicon particles, the copper atoms can be completely dissolved. The silicon solubility at this temperature is obtained from Reference 18. As long as no significant precipitation occurs, the composition of the Al-rich phase can be considered to remain equal to the one just after solid quenching.

For both the AE and the LQ + A423 specimens, the Al-rich and the Si-rich phases were shown to be present together with the θ phase. No θ' phase was detected. Therefore, the composition of the Al-rich phase is supposed to be equal to that given by the equilibrium solvus of the Al-Cu-Si system at the extrusion (for AE) or aging (for LQ + A423) temperature.

By applying Eq. [14], it follows that the measured change of the Al-rich phase lattice parameter on aging stems largely from the simultaneous precipitation of silicon and copper atoms. The beginning of the increase of the Al-rich phase lattice parameter during aging of the SQ specimens coincides with the detection of θ' phase (*cf.* Table I and Figure 2). This phase remained present during the entire range of aging times. The equilibrium θ phase was detected at the very end of the aging when the Al-rich phase lattice parameter had reached a stationary value (*cf.* Table I and Figure 2). Therefore, it can reasonably be assumed that x_{Cu} at the end of the aging times applied can be obtained from the θ'-phase solvus. Since, after aging, x_{Si} at these temperatures can be neglected, the θ'-phase solvus in the Al-Cu system is used to obtain the value of x_{Cu} at the end of the aging times applied.[17]

On the basis of the foregoing, the values of the Al-rich phase lattice parameter for specimens free of thermal stress, dependent only on x_{Si} and x_{Cu}, a^d_{Al}, are calculated and gathered in Table III. The misfit stresses resulting from thermal misfit after heat treatment are expected to exert a significant influence on the Al-rich phase lattice parameter (*e.g.*, Reference 13). The magnitude of this effect is equal to

$$\Delta a^m_{Al} = a^e_{Al} - a^d_{Al} \qquad [15]$$

where a^e_{Al} is the experimentally obtained Al-rich phase lattice parameter. The values for Δa^m_{Al} thus obtained are presented in Table III.

It is noted that at each of the three aging temperatures applied, the thermal misfit effects before and after precipitation are equal within the experimental error. This gives a further indication that the calculations of the effects of dissolved atoms on the Al-rich phase lattice parameter are correct and that the effect of misfitting θ/θ'-phase particles on the lattice parameter is negligible (Section C).

Below the eutectic temperature the solid solubility of Al in the Si-rich phase in binary Al-Si is less than 10^{-5}.[18] The maximum solid solubility of Cu in the Si-rich phase in binary Si-Cu is about 2×10^{-5}.[19] These amounts of atoms dissolved in the Si-rich phase are too small to cause any measurable change in the lattice parameter of the Si-rich phase. Also in the ternary system the solubilities of Al and Cu in the Si-rich phase are negligible.[20] Thus, the lattice parameter of the Si-rich phase is not influenced by dissolved atoms.

C. *Comparison of Observed Thermal Misfit Strains with Model Predictions*

1. *Introduction*

In the present alloy, the products of CTE and volume fractions of θ' or θ phase are too small to cause a significant lattice parameter change.[21] As the volume fraction of Si particles precipitating during aging is negligible compared to the volume fraction of Si particles already present, the contribution of precipitated Si particles to the image stress can also be neglected.

Finite element analysis of misfit stresses in a two-dimensional aluminum-based composite with inclusions of a size similar to the Si particles in our alloy indicates that disturbance of the average hydrostatic stress at the surface occurs in a layer of about 7 μm.[22] The penetration depth of X-rays in aluminum is much larger, and the effect of surface relaxation on the stresses determined by X-ray diffraction is about 2 pct.[22] Considering the accuracy of our lattice parameter determinations, surface relaxation effects are negligible.[23]

For the LQ + A423 specimen, the penetration depth of the Cu K_α X-rays in aluminum (about 75 μm) is larger than the thickness of the specimen (about 50 μm). Hence, the value of Δa^m_{Al} calculated for this specimen is, in close approximation, the average over the entire specimen. One might suggest that variations of (the hydrostatic component of) the stresses over a range of about 100 to 200 μm below the surface of the SQ + A specimens, for which the diameter (500 μm) is much larger than the penetration depth of the X-rays, can significantly influence the measured lattice parameters. However, the fact that Δa^m_{Al} calculated for the LQ + A423 specimen is within experimental error equal to the one calculated for the SQ + A423 specimen (Table III) indicates that also for SQ + A specimens, the long range variations of the stresses (if present) do not significantly influence the lattice parameters.

Thus, the lattice parameter shifts caused by the thermal misfit stresses, Δa^m_{Al}, can be obtained directly from the image stress and the bulk moduli. For the elastically deforming part of the matrix, it holds that

$$\frac{\Delta a^m_A}{a_A} = \frac{p^i}{3K_A} \qquad [16]$$

The stress in the inclusion is the sum of the image stress and pB. Hence, it holds:

$$\frac{\Delta a^m_B}{a_B} = \frac{p_B + p^i}{3K_B} \qquad [17]$$

A problem in the evaluation of the formulas for the misfit stresses is the anisotropy of aluminum and silicon. The theory described in Section A, which is based on noninteracting stress fields and isotropy of inclusions and matrix, predicts that the inclusions are in a state of hydrostatic stress. In that case, the strains in the Si particles are determined solely by the S_{11} and S_{12} elastic compliancies of the Si inclusion. Interaction of stress fields and anisotropy of the phases in the alloy will cause

Table III. Lattice Parameters of the Al-Rich Phase as Measured (a^e_{Al}) and as Calculated for Strain Free Specimens (a^d_{Al})*

Heat Treatment	ΔT (K)	x_{Cu} $\times(10^2)$	x_{Si} $\times(10^2)$	Al-Rich Phase Lattice Parameter		
				a^d_{Al} (nm)	a^e_{Al} (nm)	Δa^m_{Al} (pm)
LQ + A423, t = 700 h	130	0.01	0	0.40496	0.40516	0.20
AE	360	0.5	0.2	0.40469	0.40495	0.26
SQ/RT	500	1.59	1.05	0.40402	0.40428	0.26
SQ + A423, t < 1 h	130	1.59	1.05	0.40402	0.40421	0.19
SQ + A453, t < 0.3 h	160	1.59	1.05	0.40402	0.40424	0.22
SQ + A483, t < 0.1 h	190	1.59	1.05	0.40402	0.40431	0.29
SQ + A423, t > 200 h	130	0.11	0	0.40490	0.40510	0.20
SQ + A453, t > 100 h	160	0.15	0	0.40489	0.40512	0.23
SQ + A483, t > 10 h	190	0.27	0	0.40483	0.40511	0.28

*The difference, Δa^m_{Al}, is ascribed to thermal misfit.

deviations from the pure hydrostatic stress state in the inclusions. Providing that these disturbances are small, it is justified to obtain the elastic constants of the Si inclusions from the S_{11} and S_{12} compliancies.[11] The anisotropy of aluminum is relatively small. For this reason, the elastic constants of polycrystalline aluminum are used for the calculations.[11] The yield strength of the Al-1.3 at. pct Cu-19.1 at. pct Si alloy was estimated to be equal to the yield strength of an Al-1.6 at. pct Cu in the T4 condition (200 MPa).[20] The relevant material property values are gathered in Table IV.

The effect of variations in the yield strength on lattice parameter values is shown in Figure 4. In this figure, values of $\Delta a_{pl}/\Delta a_{el}$, where Δa_{pl} is the lattice parameter shift calculated with the elastic-plastic model and Δa_{el} is the lattice parameter shift calculated with the elastic model, are given as a function of the yield strength of the matrix for ΔT = 153 K. In the case of plastic accommodation (Eqs. [9] through [13] and [16]), the average lattice parameters of the elastically deformed part of the matrix and of the plastically deformed part of the matrix are different. Hence, in Figure 4, three values of $\Delta a_{pl}/\Delta a_{el}$ are given for the matrix: one for the elastically deformed part, one for the plastically deformed part, and an average value of $\Delta a_{pl}/\Delta a_{el}$, as obtained from the average volume change of the entire matrix (plastically and elastically deformed zones).* As plastic deformation will not occur in the inclusions (they are in a hydrostatic stress state), only one value of $\Delta a_{pl}/\Delta a_{el}$ is given for the inclusions. From the calculations, it follows that for σ_y < 100 MPa, overlap of the plastic zones occurs, which might limit the applicability of the model.

Figure 4 shows that the lattice parameter of both the elastically deformed zone and the average lattice parameter of the matrix vary only slightly when the yield strength is varied around the value of 200 MPa. Hence, an inaccurate estimation of the yield strength of the matrix has only limited influence on calculated Al-rich phase lattice parameters. Figure 4 also demonstrates that the yield strength of the matrix has a profound influence on the lattice parameter shift of the inclusion.

2. *The Al-rich phase lattice parameter*

In Figure 5, the experimental values for $\Delta a^m_{Al}/a_{Al}$ (Section B) are plotted as a function of the temperature drop ΔT. The values for pure elastic accommodation (obtained from Eqs. [3] through [5] and [16] are represented by the straight line through the origin (line A). For the case of elastic/plastic accommodation, line B gives $\Delta a^m_{Al}/a_{Al}$ for the elastically deforming part of the matrix (representing the maximal lattice parameter shift possible at any location in the matrix). Line C gives the average value of $\Delta a^m_{Al}/a_{Al}$ as obtained from the average

Table IV. Coefficients of Thermal Expansion, Elastic Constants, and Yield Strength

	α (10^{-6} K^{-1})	K (GPa)	μ (GPa)	σ_y (MPa)
Matrix	23.5	69	27	200
Si phase	3.0	99	51	—

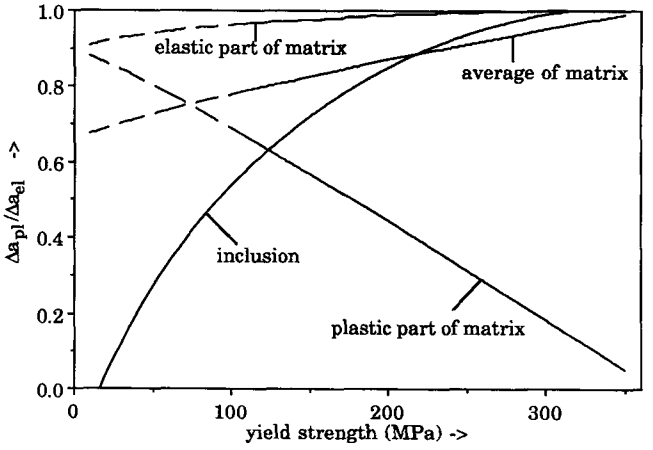

Fig. 4 — The lattice parameter shifts calculated with the elastic-plastic model divided by those for the elastic model as a function of the yield strength of the matrix for ΔT = 153 K: (1) the value for the elastically deforming part of the matrix (only influenced by p_i); (2) the value for the plastically deforming part of the matrix (as obtained from the average volume change of that part of the matrix); (3) the average value for the matrix (as obtained from the average volume change of the matrix); and (4) the value for the inclusion.

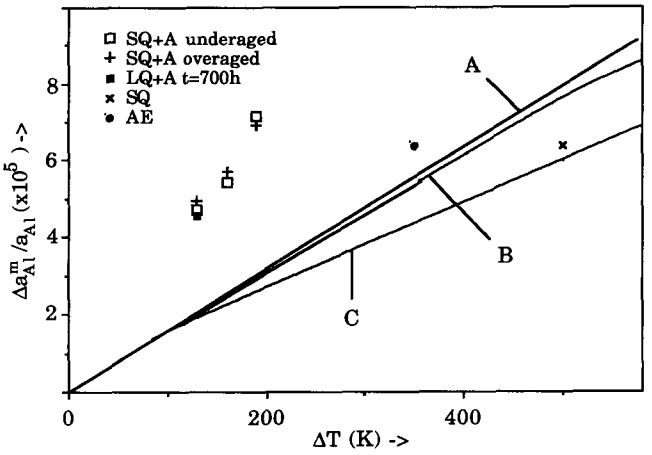

Fig. 5—Measured data (Table III) and model predictions of the lattice parameter shift of the Al-rich phase due to accommodation of thermal misfit. Line A gives the lattice parameter shift for the case of pure elastic accommodation. For the case of elastic/plastic accommodation, both the lattice parameter shift of the elastically deforming part of the matrix (line B) and the average lattice parameter shift of the matrix (line C) are given. For $\Delta T < 84$ K, no plastic accommodation occurs according to the von Mises criterion.

volume change of the entire matrix (plastically and elastically deformed zones).*

*It should be noted that this calculation of the lattice parameter shift for the matrix implicitly assumes that the centroid and the peak position of a diffracted line are situated at the same diffraction angle. Available experimental evidence[24] indicates that possible effects are negligibly small.

It is observed that the measured value of $\Delta a^m_{Al}/a_{Al}$ for the SQ specimen corresponds fairly well with the theoretical predictions for plastic/elastic accommodation. The value for the AE specimen is rather larger than the predicted value for plastic/elastic accommodation, whereas the values for aged specimens are much larger than the theoretical predictions for both models. For these low values of ΔT, $\Delta a^m_{Al}/a_{Al}$ appears to be proportional to ΔT. Alternatively, one could suggest that if the observed deviations from the model predictions are related with a deviation from ideal plastic behavior of the matrix, $\Delta a^m_{Al}/a_{Al}$ for ΔT lower than 84 K (where according to the von Mises criterion, only elastic accommodation occurs) would correspond to the model prediction for elastic accommodation. To clarify this point, additional DbS experiments were performed on a specimen that was aged for 4, 24, and 200 hours at 365 K and subsequently quenched in water. For these experiments, the specimen which was previously aged for 512 hours at 453 K was chosen. The additional aging at 365 K failed to produce any significant changes in either the Al-rich phase or the Si-phase lattice parameter. Apparently, this aging temperature is too low to relieve the stress state that was introduced by cooling from the initial aging temperature (453 K), and after subsequent cooling to room temperature, this stress state was restored.

It is assumed that the value of the average hydrostatic stress is not influenced by the weak texture or by elastic anisotropy. As the radius of the deformed zone around the inclusion is on the order of 1.2 to 1.5 times the radius of the inclusion (about 2 μm) while the grainsize is about 10 μm, only a very small volume fraction of the plastically deformed zones is influenced by grain boundaries. Hence, the overwhelming majority of the dislocations created due to thermal misfit is not affected by grain boundaries, and it is assumed that grain size does not influence the misfit stresses.

Van Berkum *et al.*[25] studied the relaxation of stresses in Al-Si alloys which were cooled to room temperature after aging at 453 K. It was found that about 50 pct of the lattice parameter shift due to thermal misfit stresses is relaxed in 12 years aging at room temperature (full relaxation was not observed within the longest natural aging time studied (12 years)). Assuming an activation energy for dislocation movement of about 1.2 eV,[26] it can be shown that relaxation at the aging temperatures applied occurs within a few minutes. These estimated relaxation times are in agreement with the Si-rich phase lattice parameters during aging (Figure 3), which reach a stationary value that is different from the one after quenching within the first aging interval of 3.75 minutes. Hence, it is unlikely that the Al-rich phase lattice parameters after aging are influenced by the dislocations created on quenching.

For several Al-based composites, the predictions of Eshelby-type models (*e.g.*, References 27 and 28) for the stress in matrices due to elastic misfit accommodation are also lower than the measured stresses.[29–32] Application of the von Mises criterion indicates that plastic accommodation occurred for the cases reported. Application of the present model for elastic/plastic accommodation of misfitting spherical inclusions in a finite matrix yields lattice parameter shifts which are smaller than in the case of pure elastic accommodation. Hence, application of the present model enlarges the discrepancies between model predictions and measured stresses.

It can be shown that the observed lattice parameter shifts are within the limits given by the requirement of conservation of energy.[21] In other words, the energy released due to plastic relaxation is sufficiently large to provide the elastic energy of the observed image stresses. This would imply that during plastic relaxation, the energy related to microstresses (*i.e.*, short-range stresses around misfitting Si particles) is reduced while the energy related to macrostress (*i.e.*, the long-range stress which determines the average lattice parameter) is increased. An indication that the transfer of energy associated with the microstresses to energy associated with the macrostress during the creation of defects in the plastically deformed zone, as suggested earlier, can occur in composites is found in work by Mittemeijer and coworkers.[25,29] They have shown that in Al-Si alloys quenched from 447 K to room temperature, the average macrostrain is larger than the model predictions based on pure elastic accommodation while the microstrains are lower than predictions based on the same model.

As the observed positive deviation of the image stresses from the theoretical predictions can only be related to additional misfit, the preceding discussion suggests that the average volume of the plastically deformed

zone is increased as a result of plastic deformation, causing additional misfit. Hence, defects created in the plastic zone (for instance, dislocations, vacancies, and subgrains[33]) are expected to increase the average volume of this zone.*

*It is well known that dislocations and vacancies increase the specific volume of metals.[34,35] Volume changes observed after plastic deformation in uniaxial tensile experiments, however, are too small to explain the observed effects in our alloy. This may be due to the different spatial arrangement of the defects. Further, it is noted that the plastically deformed zone around misfitting inclusions in a composite is in a complex triaxial stress state, which may interact with the defects present in this zone. In contrast, a piece of material which is plastically deformed in a uniaxial tensile test is nearly stress free after removal of the applied force.

Up to this point, it has been assumed that during aging the specimens are free of thermal stress. This assumption is supported by the data on room-temperature stress relaxation of van Berkum *et al.*[25] discussed earlier. However, aging of plastically deformed metals can partly annihilate the dislocations introduced by plastic deformation but may not eliminate the plastic deformation itself. Hence, it is conceivable that the plastic strains introduced by solid quenching are, at least partly, retained during aging. Then these retained plastic strains can influence the stress state after cooling from the aging temperature. In an extreme case, heating to the aging temperature, aging and subsequent cooling to room temperature do not alter the stress state at all, and as a consequence, the stress state present after solid quenching is restored after aging. This can explain why the Al-rich phase lattice parameter shifts due to thermal misfit stresses after aging are quite close to the one after solid quenching (all shifts are in the range 4.5 to 7 $\times$ 10^{-5} a_{Al}; Figure 5). It can even explain why aging at 365 K failed to produce any changes in either the Al-rich or the Si-rich phase lattice parameter, as discussed previously. Of course, this does not totally exclude the possibility of stress relaxation during aging. For instance, the sharp change of the Si-rich phase lattice parameter after 3.75 minutes aging as compared to the Si-rich phase lattice parameter after solid quenching (*cf.* Figure 3 and Table II) indicates relaxation of stresses around Si particles.

3. *The Si-rich phase lattice parameter*

In Figure 6, the values for the thermal misfit effect on the Si-rich phase lattice parameter based on the theory for elastic and for elastic/plastic accommodation (Eqs. [9] through [13] and [17]) are compared with the experimentally observed values. It is observed that the lattice parameter shifts predicted by the elastic model are significantly larger than the observed values. The calculated values for the elastic/plastic model correspond reasonably well to the observed values.

Since the amount of atoms that can be dissolved in the Si-rich phase is too small to cause any measurable change in the lattice parameter of this phase, deviations of the Si-rich phase lattice parameter from the value for pure, unstrained Si can only be caused by stresses. The Si-rich phase lattice parameter after solid quenching and subsequent storage in liquid nitrogen is close to the value for pure unstrained Si (Table II), whereas the value after solid quenching is much lower than the value for pure unstrained Si. As the elastic stresses in the inclusion are balanced by the elastic stresses in the Al-rich matrix, the Al-rich phase lattice parameter should decrease due to the storage in nitrogen. This is indeed observed (Table II). Ericsson *et al.*[36] observed that quenching in liquid nitrogen reduces the internal stresses in the Al-rich phase of a 6061 aluminum alloy reinforced with SiC whiskers by about 70 pct as compared to quenching in water at room temperature. Since the CTE of SiC, like the CTE of Si, is also much lower than the CTE of Al, this reduction of stresses is thought to stem from the same causes.

In attempting to explain the observed effect of storage in liquid nitrogen, it is first noted that the theory incorporating plastic accommodation as given in Section A cannot be used in this case, since (1) large overlap of plastic zones is expected to occur, and (2) the theory does not predict stresses and plastic strains for the case of multiple temperature changes of opposite sign. Figure 6 shows that directly after solid quenching (ΔT = 500 K), the absolute value of the lattice parameter shift of the Si-rich phase is much smaller than the predictions based on the theory for pure elastic accommodation. This indicates plastic deformation of the matrix. On quenching specimens in liquid nitrogen, the thermal misfit at the storage temperature is increased. The theory for elastic/plastic accommodation indicates that this increase in misfit leaves Δa_{Si} nearly unchanged (Figure 6). Hence, the additional misfit is mainly accommodated by plastic deformation of the Al-rich phase. When, after the storage period, the temperature of these specimens is increased to room temperature, the misfit parameter is equal to the one in the quenched specimens which were stored at room temperature. However, plastic deformation introduced by quenching in liquid nitrogen can reduce the need for elastic accommodation. In fact, the Si-rich phase lattice parameter determined after storage in liquid nitrogen indicates that nearly no elastic deformation is present in the Si particles.

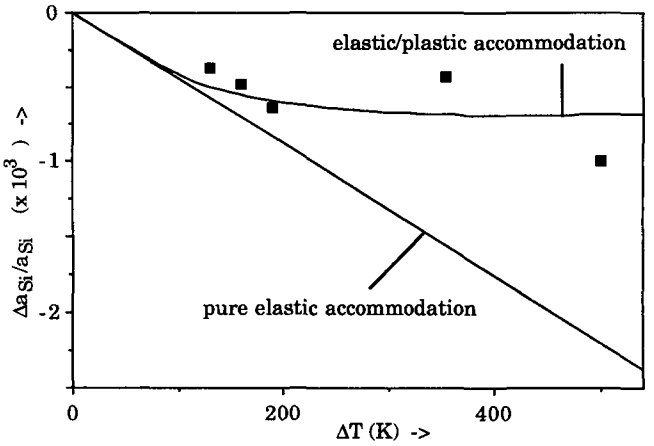

Fig. 6—Comparison of measured $\Delta a_{Si}/a_{Si}$ values with theoretical predictions for the Al-1.3 at. pct Cu-19.1 at. pct Si alloy. For the SQ + A specimens (ΔT < 200 K), the average Si-rich phase lattice parameter shift during aging is given.

V. CONCLUSIONS

X-ray diffraction on Al-Cu-Si alloys showed the following.

1. For the homogenized Al-1.07 at. pct Cu-1.01 at. pct Si alloy, the effects of dissolved Cu and Si atoms on the lattice parameter of the Al-rich phase are independent and additive.
2. During aging after solid quenching of Al-1.3 at. pct Cu-19.1 at. pct Si alloys, the Al-rich phase lattice parameter, which is initially lower than value for pure, unstrained Al, increases due to precipitation of Si and Cu atoms.
3. The model describing the stress state around a single misfitting spherical inclusion in an infinite matrix which shows ideal plastic behavior, as given by Lee *et al.*[14] is extended to describe the stress state in a finite composite. This model predicts an average hydrostatic stress in the matrix which is somewhat lower than in the case of pure elastic accommodation.
4. This model describes the measured lattice parameter shifts of the Si phase reasonably well.
5. Comparison of the model incorporating elastic accommodation and the model incorporating ideal plastic accommodation with measured stresses shows a good correspondence for the Al-rich phase lattice parameter of solid-quenched specimens. For specimens quenched after aging, significant discrepancies remain.
6. Elastic stresses in the solid-quenched Al-1.3 at. pct Cu-19.1 at. pct Si alloy at room temperature are reduced by quenching in liquid nitrogen.

ACKNOWLEDGMENTS

The authors are indebted to Messrs. P. de Ruiter and H. Kleinjan for providing the melt-spun alloy, to Drs. J. Duszczyk and Zhou Jie for performing the extrusion, and to Ing. N.M. van der Pers and Mr. J.F. van Lent for assistance with the X-ray diffraction experiments.

The financial support of the Foundation for Fundamental Research of Matter and for Technological Sciences (FOM/STW) is gratefully acknowledged.

REFERENCES

1. J.A. van der Hoeven, P. van Mourik, and E.J. Mittemeijer: *J. Mater. Sci. Lett.*, 1983, vol. 18, pp. 158-60.
2. D. Bialo, J. Duszczyk, A.W.J. de Gee, G.J.J. van Heijningen, and B.M. Korevaar: *Wear*, 1991, vol. 141, pp. 291-309.
3. T. Christman and S. Suresh: *Acta Metall.*, 1988, vol. 36, pp. 1691-1704.
4. J.M. Papazian: *Metall. Trans. A*, 1988, vol. 19, pp. 2945-53.
5. I. Dutta, S.M. Allen, and J.F. Hafley: *Metall. Trans. A*, 1991, vol. 22A, pp. 2553-63.
6. M.J. Starink, V. Jooris, and P. van Mourik: *Proc. 12th RISØ Int. Symp. on Metal Matrix Composites—Processing, Microstructure and Properties*, Roskilde, Denmark, Sept. 2–6, 1991, N. Hansen, D. Juul Jensen, T. Leffers, H. Lilholt, T. Lorentzen, A.S. Pedersen, O.B. Pedersen, and B. Ralph, eds., RISØ National Laboratory, Roskilde, Denmark, 1991, pp. 675-82.
7. M. Taya, K.E. Lulay, and D.J. Lloyd: *Acta Metall. Mater.*, 1991, vol. 39, pp. 73-87.
8. P.B. Prangnell and W.M. Stobbs: *Proc. 12th RISØ Int. Symp. on Metal Matrix Composites—Processing, Microstructure and Properties*, Roskilde, Denmark, Sept. 2–6, 1991, N. Hansen, D. Juul Jensen, T. Leffers, H. Lilholt, T. Lorentzen, A.S. Pedersen, O.B. Pedersen, and B. Ralph, eds., RISØ National Laboratory, Roskilde, Denmark, 1991, pp. 603-10.
9. M.J. Starink and P. van Mourik: *Metall. Trans. A*, 1991, vol. 22A, pp. 665-74.
10. B.D. Cullity: *Elements of X-ray diffraction*, 2nd ed., Addison-Wesley, Reading, MA, 1978.
11. *Metals Reference Book*, 5th ed., C.J. Smithells, ed., Butterworth's, London, 1976.
12. W.B. Pearson: *Handbook of Lattice Spacings and Structures of Metals and Alloys*, Pergamon Press, London, 1967, vol. II.
13. P. van Mourik, E.J. Mittemeijer, and Th.H. de Keijser: *J. Mater. Sci.*, 1983, vol. 18, pp. 2706-20.
14. J.K. Lee, Y.Y. Earmme, H.I. Aaronson, and K.C. Russell: *Metall. Trans. A*, 1980, vol. 11A, pp. 1837-47.
15. M.J. Starink and P.J. van Mourik: *Mater. Sci. Eng.*, 1992, vol. 156A, pp. 183-94.
16. T.B. Massalski: *Physical Metallurgy*, 3rd ed., R.W. Cahn and P. Haasen, eds., Elsevier, New York, NY, 1983, pp. 153-218.
17. J.L. Murray: *Int. Metall. Rev.*, 1985, vol. 30, pp. 211-33.
18. J.L. Murray and A.J. McAlister: *Bull. Alloy Phase Diag.*, 1984, vol. 5, pp. 74-84.
19. R.W. Olesinski and G.J. Abbaschian: *Bull. Alloy Phase Diag.*, 1986, vol. 7, pp. 170-78.
20. L.F. Mondolfo: *Aluminum Alloys: Structure and Properties*, Butterworth's, London, 1976.
21. M.J. Starink: Ph.D. Thesis, Delft University of Technology, Delft, The Netherlands, 1992.
22. Li Shouxin, Sun Lizhi, Sue Zhengming, and Wang Zhongguang: *Scripta Metall. Mater.*, 1991, vol. 25, pp. 2431-34.
23. R.D. Mindlin and D.H. Cheng: *J. Appl. Phys.*, 1950, vol. 21, pp. 931-33.
24. J.G.M. van Berkum, R. Delhez, Th.H. de Keijser, and E.J. Mittemeijer: *Phys. Stat. Sol.*, 1992, vol. 134, pp. 335-50.
25. J.G.M. van Berkum, R. Delhez, Th.H. de Keijser, E.J. Mittemeijer, and P. van Mourik: *Scripta Metall. Mater.*, 1991, vol. 25, pp. 2255-58.
26. P. van Mourik, Th.H. de Keijser, and E.J. Mittemeijer: *Scripta Metall.*, 1987, vol. 21, pp. 381-85.
27. J.D. Eshelby: *Progress in Solid Mechanics*, I.N. Sneddon and R. Hill, eds., North-Holland, Amsterdam, 1961, vol. 2, pp. 88-140.
28. P.J. Whithers, W.M. Stobbs, and O.B. Pedersen: *Acta Metall.*, 1989, vol. 37, pp. 3061-84.
29. E.J. Mittemeijer, P. van Mourik, and Th.H. de Keijser: *Phil. Mag. A*, 1981, vol. 43, pp. 1157-64.
30. M.J. Starink, V. Abeels, and P. van Mourik: *Mater. Sci. Eng.*, in press.
31. H.M. Ledbetter and M.W. Austin: *Mater. Sci. Eng.*, 1987, vol. 89, pp. 53-61.
32. M. Taya and R.J. Arsenault: *Metal Matrix Composites—Thermomechanical Behavior*, Pergamon Press, Oxford, 1989, pp. 106-09.
33. H.G. van Buren: *Acta Metall.*, 1955, vol. 3, pp. 519-24.
34. R. Vetter, R.H.J. Fastenau, and M.I. Baskes: *Phys. Stat. Sol. A*, 1981, vol. 67, pp. 585-89.
35. A. Loyer and J.M. Dorlot: *Phys. Stat. Sol. A*, 1970, vol. 2, pp. 91-99.
36. T. Ericsson, C. Persson, and A. Ohlson: *Proc. 12th RISØ Int. Symp. on Metal Matrix Composites—Processing, Microstructure and Properties*, Roskilde, Denmark, Sept. 2–6, 1991, N. Hansen, D. Juul Jensen, T. Leffers, H. Lilholt, T. Lorentzen, A.S. Pedersen, O.B. Pedersen, and B. Ralph, eds., RISØ National Laboratory, Roskilde, Denmark, 1991, pp. 329-35.